

Continuous variable quantum teleportation using photon subtracted and photon added two mode squeezed coherent state

Shikhar Arora,^{1,*} Chandan Kumar,^{1,†} and Arvind^{1,‡}

¹*Department of Physical Sciences, Indian Institute of Science Education and Research Mohali, Sector 81 SAS Nagar, Punjab 140306 India.*

We consider non-Gaussian states generated by photon subtraction (PS) and photon addition (PA) on two-mode squeezed coherent (TMSC) states, as resource states for continuous variable (CV) quantum teleportation (QT). To this end, we derive the Wigner characteristic function for the family of photon subtracted and photon added TMSC states, which is then utilized to calculate the fidelity of teleporting a single mode coherent state and a squeezed vacuum state. The analysis shows that while symmetric PS enhances the fidelity of QT in an extensive range of squeezing, asymmetric PS enhances the performance marginally and only in the low squeezing regime. The addition operations on the other hand are less useful, symmetric three-PA leads to a marginal improvement while the other addition operations are useless. We have considered the actual experimental setup for PS and PA operations and computed their success probabilities which should be kept in mind while advocating the use of these operations. We could compute the fidelity of QT for a broad range of states because we analytically derived the Wigner characteristic function for these family of states which we think will be useful for various other applications of these families of states.

I. INTRODUCTION

The non-classical subset of, two mode Gaussian states, in particular, two mode squeezed vacuum (TMSV) state, have played a crucial role in the development of various continuous variable (CV) quantum information processing (QIP) protocols, for instance, quantum teleportation [1], entanglement swapping [2], and quantum key distribution [3]. However, in recent times, much attention is being paid to non-Gaussian states, which are generated using non-Gaussian operations such as photon subtraction (PS) and photon addition (PA) on initial Gaussian states [4]. These non-Gaussian operations can enhance the nonclassicality [5] and entanglement content of the state that they act upon [6–10]. Non-Gaussian operations have already been considered for performance enhancement in quantum illumination [11–15], quantum teleportation (QT) [16–25] and quantum metrology [26–33]. Furthermore, non-Gaussian operations have been utilized in loophole-free tests of Bells inequality [34, 35] and in quantum computing [36].

While dealing with Gaussian states and Gaussian operations is theoretically simple, calculations involving non-Gaussian states and non-Gaussian operations can be complicated. This poses a formidable challenge to analyzing non-Gaussian operations, even on simple Gaussian states. The PS and PA operations on TMSV states have been extensively studied in quantum teleportation, whereas PS and PA operations on more general class of Gaussian states such as two mode squeezed coherent (TMSC) states are unexplored. This can be attributed mainly to challenges involved in the mathematical de-

scription of these general non-Gaussian states and in calculating the quantities of interest such as QT fidelity.

It should be noted that PS and PA are probabilistic processes, and therefore, the success probability must be taken into account while analyzing any quantity of interest. However, most previous research has considered ideal PS and PA operations via the annihilation and creation operators and ignored the success probability entirely. To account for the success probability, one needs to consider the practical scheme for non-Gaussian operations, which results in additional parameters. For instance, transmissivity parameters are included while considering the PS operation modeled using a beam splitter. This additional parameter further increases the challenge of working out an analytical solution.

This work considers non-Gaussian states generated by realistic PS and PA operations on TMSC state as resource states for CV QT. TMSC state can be easily generated in a lab by feeding coherent state to a parametric down converter [37]. TMSC states have already been studied in detail [38, 39] and recently, theoretical analysis was undertaken in the context of quantum metrology [37]. Here we endeavor to explore whether the state generated by PS and PA operations on TMSC state when used as resource states can yield higher fidelity of QT. To this end, we first derive the Wigner characteristic functions of the PSTMSC and PATMSC states in terms of two-variable Hermite polynomials. These functions have the transmissivity of the two beam splitters as parameters, and by suitably choosing the transmissivity, we can perform asymmetric and symmetric PS and PA operations. We then derive the fidelity of QT for an input coherent state and squeezed vacuum state. Since we have considered practical models for PS and PA operations, we take the success probability of the respective non-Gaussian operations into account while analyzing the fidelity of QT.

The results show that symmetric PS operations en-

* shikhar.quantum@gmail.com

† chandan.quantum@gmail.com

‡ arvind@iisermohali.ac.in

hance the fidelity of QT. However, for the asymmetric PS operations, the enhancement is seen only in the low squeezing range. We note that the success probability for symmetric n -PS is less when compared to asymmetric n -PS. Among the PA operations, symmetric 3-PA, whose success probability is very low, slightly improves the fidelity of QT for an input squeezed vacuum state. For all other cases, the PA operation is not useful. We were able to carry out fidelity calculations because we managed to compute the the Wigner characteristic function for the PSTMSC and PATMSC states which we think would be valuable in characterizing these states and to analyse their use in various QIP tasks.

The paper is organized as follows. In Sec. II, we derive the Wigner characteristic functions of the PSTMSC and PATMSC states. In Sec III, we derive the fidelity of teleportation for an input coherent state and squeezed vacuum state and analyze them. Finally, in Sec. IV, we provide some concluding remarks and discuss future directions. In Appendix A, we provide a brief overview of CV systems and their phase space representation.

II. WIGNER CHARACTERISTIC FUNCTION OF PSTMSC AND PATMSC STATES

We first derive the Wigner characteristic function of the PSTMSC state. The schematic for the generation of

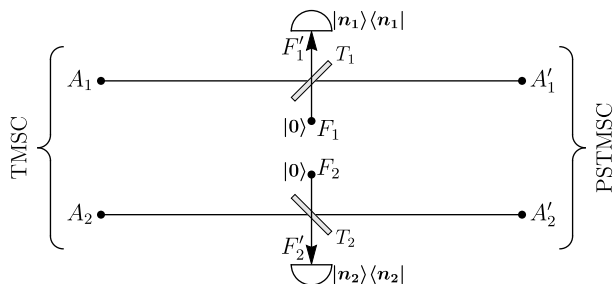


FIG. 1. Scheme for the preparation of PSTMSC state. Modes A_1 and A_2 of TMSC state are mixed with modes F_1 and F_2 , initialized to vacuum states, using beam splitter of transmissivity T_1 and T_2 , respectively. Photon number resolving detectors (PNRD) given by the POVM $\{|n_1\rangle\langle n_1|, \mathbb{1} - |n_1\rangle\langle n_1|\}$ and $\{|n_2\rangle\langle n_2|, \mathbb{1} - |n_2\rangle\langle n_2|\}$ are applied to modes F_1' and F_2' respectively. Simultaneous click of the POVM elements $|n_1\rangle\langle n_1|$ and $|n_2\rangle\langle n_2|$ represents successful subtraction of n_1 and n_2 photons from the modes A_1 and A_2 of the TMSC state, respectively.

the PSTMSC state is shown in Fig. 1. We start with an uncorrelated two mode coherent state given by

$$|\psi\rangle_{A_1 A_2} = D_{A_1}(d, d) D_{A_2}(d, d) |00\rangle, \quad (1)$$

where $D_i(d, d)$ is the displacement operator defined in Eq. (A5) of the Appendix A. Since two-mode coherent state is a Gaussian state, the Wigner characteristic func-

tion can be written using Eq. (A20) as

$$\chi(\Lambda) = \exp \left[- \frac{\tau_1^2 + \sigma_1^2 + \tau_2^2 + \sigma_2^2}{4} \right. \\ \left. + i(\sigma_1 + \sigma_2) d - i(\tau_1 + \tau_2) d \right]. \quad (2)$$

The TMSC state is generated by sending two-mode coherent state through a non-linear optical down converter [37]:

$$|\Psi\rangle_{A_1 A_2} = \mathcal{U}(S_{A_1 A_2}(r)) |\psi\rangle_{A_1 A_2}, \quad (3)$$

where $\mathcal{U}(S_{A_1 A_2}(r))$ is the two mode squeezing operation defined in Eq. (A12) of the Appendix A. The Wigner characteristic function transforms as $\chi(\Lambda) \rightarrow \chi(S_{A_1 A_2}^{-1}(r)\Lambda)$, which evaluates to

$$\chi_{A_1 A_2}(\Lambda) = \exp \left[i(\sigma_1 + \sigma_2) d e^r - i(\tau_1 + \tau_2) d e^{-r} \right. \\ \left. - \frac{\tau_1^2 + \sigma_1^2 + \tau_2^2 + \sigma_2^2}{4} \cosh(2r) + \frac{\tau_1 \tau_2 - \sigma_1 \sigma_2}{2} \sinh(2r) \right]. \quad (4)$$

We combine the modes A_1 and A_2 of the TMSC state with ancilla modes F_1 and F_2 , initiated to vacuum states using beam-splitters of transmissivity T_1 and T_2 respectively. We represent the modes A_1 and A_2 by the quadrature operators $(\hat{q}_1, \hat{p}_1)^T$ and $(\hat{q}_2, \hat{p}_2)^T$, and the ancilla modes F_1 and F_2 by the quadrature operators $(\hat{q}_3, \hat{p}_3)^T$ and $(\hat{q}_4, \hat{p}_4)^T$, respectively. The characteristic function of the four mode system before the beam splitter operations can be written as

$$\chi_{F_1 A_1 A_2 F_2}(\Lambda) = \chi_{A_1 A_2}(\Lambda) \chi_{|0\rangle}(\Lambda_3) \chi_{|0\rangle}(\Lambda_4), \quad (5)$$

where $\chi_{|0\rangle}(\Lambda_i)$ ($i = 3, 4$) is the Wigner characteristic function of the vacuum state. The four modes get entangled as a result of mixing by the two beam splitters $B(T_1, T_2) = B_{A_1 F_1}(T_1) \oplus B_{A_2 F_2}(T_2)$, where $B_{ij}(T)$ is beam splitter operation defined in Eq. (A9) of the Appendix A. The transformed characteristic function can be calculated as

$$\chi_{F_1' A_1' A_2' F_2'}(\Lambda) = \chi_{F_1 A_1 A_2 F_2}(B(T_1, T_2)^{-1}\Lambda). \quad (6)$$

The modes F_1' and F_2' are measured with photon number resolving detectors (PNRD) represented by the positive-operator-valued measure (POVM) $\{\Pi_{n_1} = |n_1\rangle\langle n_1|, \mathbb{1} - \Pi_{n_1}\}$ and $\{\Pi_{n_2} = |n_2\rangle\langle n_2|, \mathbb{1} - \Pi_{n_2}\}$ respectively. When the POVM elements Π_{n_1} and Π_{n_2} click simultaneously, PS operation on both the modes is considered to be successful. In this paper, we consider symmetric and asymmetric PS operation. Symmetric PS corresponds to equal number of photons being detected in both the modes, *i.e.*, $n_1 = n_2 = n$. The resultant state is referred to as Sym n -PSTMSC state. Asymmetric PS corresponds to PS on one of the modes (mode A_2 in this paper). The resultant state is referred to as Asym n -PSTMSC state. The

results for Asym n -PSTMSC state can be obtained from the general expression by setting $n_1 = 0$, $n_2 = n$, and $T_1 = 1$. Post-measurement, the unnormalized Wigner characteristic function can be written as

$$\begin{aligned} \tilde{\chi}_{A'_1 A'_2}^{\text{PS}} = & \frac{1}{(2\pi)^2} \int d^2\Lambda_3 d^2\Lambda_4 \underbrace{\chi_{F'_1 A'_1 A'_2 F'_2}(\Lambda)}_{\text{Four mode entangled state}} \\ & \times \underbrace{\chi_{|n_1\rangle}(\Lambda_3)}_{\text{Projection on } |n_1\rangle\langle n_1|} \underbrace{\chi_{|n_2\rangle}(\Lambda_4)}_{\text{Projection on } |n_2\rangle\langle n_2|}, \end{aligned} \quad (7)$$

where $\chi_{|n_i\rangle}(\Lambda_i)$ ($i = 3, 4$) is the Wigner characteristic function of the Fock state $|n_i\rangle$ and can be written in terms of Laguerre polynomial as given in Eq. (A15) of the Appendix A. Integration of Eq. (7) yields

$$\begin{aligned} \tilde{\chi}_{A'_1 A'_2}^{\text{PS}} = & a_0 \exp(\mathbf{\Lambda}^T M_1 \mathbf{\Lambda} + \mathbf{\Lambda}^T M_2) \\ & \times \widehat{\mathbf{F}}_1 \exp[-a_1 u_1 v_1 + a_2 u_1 + a_3 v_1 - a_4 u_2 v_2 \\ & + a_5 u_2 + a_6 v_2 + a_7(u_1 u_2 + v_1 v_2)], \end{aligned} \quad (8)$$

where the coefficients a_i are provided in Eq. (B1) of the Appendix B, the column vector $\mathbf{\Lambda}$ is defined as $(\tau_1, \sigma_1, \tau_2, \sigma_2)^T$, and the matrices M_1 and M_2 are given in Eqs. (B3) and (B4) of the Appendix B. Further, the differential operator $\widehat{\mathbf{F}}_1$ is defined as

$$\widehat{\mathbf{F}}_1 = \frac{2^{-(n_1+n_2)}}{n_1!n_2!} \frac{\partial^{n_1}}{\partial u_1^{n_1}} \frac{\partial^{n_1}}{\partial v_1^{n_1}} \frac{\partial^{n_2}}{\partial u_2^{n_2}} \frac{\partial^{n_2}}{\partial v_2^{n_2}} \{\bullet\}_{\substack{u_1=v_1=0 \\ u_2=v_2=0}}. \quad (9)$$

Equation (8) can further be expressed in terms of two-variable Hermite polynomials $H_{m,n}(x, y)$, which has been explicitly demonstrated in Appendix B:

$$\begin{aligned} \tilde{\chi}_{A'_1 A'_2}^{\text{PS}} = & a_0 \frac{2^{-(n_1+n_2)}}{n_1!n_2!} \exp(\mathbf{\Lambda}^T M_1 \mathbf{\Lambda} + \mathbf{\Lambda}^T M_2) \\ & \times \sum_{i,j=0}^{\min(n_1, n_2)} \frac{a_1^{n_1}}{\sqrt{a_1}^{i+j}} \frac{a_4^{n_2}}{\sqrt{a_4}^{i+j}} \frac{a_7^{i+j}}{i!j!} P_i^{n_1} P_j^{n_1} P_i^{n_2} P_j^{n_2} \\ & \times H_{n_1-i, n_1-j} \left[\frac{a_2}{\sqrt{a_1}}, \frac{a_3}{\sqrt{a_1}} \right] H_{n_2-i, n_2-j} \left[\frac{a_5}{\sqrt{a_4}}, \frac{a_6}{\sqrt{a_4}} \right], \end{aligned} \quad (10)$$

where $P_r^n = n!/(n-r)!$ is r -permutation of n . We note that the afore-derived Wigner characteristic function is unnormalized. The normalization corresponds to the probability of simultaneous click of both the PNRD detectors and can be computed as follows:

$$\begin{aligned} P^{\text{PS}} = & \tilde{\chi}_{A'_1 A'_2}^{\text{PS}} \Big|_{\substack{\tau_1=\sigma_1=0 \\ \tau_2=\sigma_2=0}} = a_0 \widehat{\mathbf{F}}_1 \exp[-a_1 u_1 v_1 + b_2 u_1 \\ & + b_3 v_1 - a_4 u_2 v_2 + b_5 u_2 + b_6 v_2 + a_7(u_1 u_2 + v_1 v_2)], \end{aligned} \quad (11)$$

where the coefficients b_i are provided in Eq. (B2) of the Appendix B. Equation (11) can also be expressed

in terms of two-variable Hermite polynomials as

$$\begin{aligned} P^{\text{PS}} = & a_0 \frac{2^{-(n_1+n_2)}}{n_1!n_2!} \sum_{i,j=0}^{\min(n_1, n_2)} \frac{a_1^{n_1}}{\sqrt{a_1}^{i+j}} \frac{a_4^{n_2}}{\sqrt{a_4}^{i+j}} \frac{a_7^{i+j}}{i!j!} P_i^{n_1} \\ & \times P_j^{n_1} P_i^{n_2} P_j^{n_2} H_{n_1-i, n_1-j} \left[\frac{b_2}{\sqrt{a_1}}, \frac{b_3}{\sqrt{a_1}} \right] H_{n_2-i, n_2-j} \left[\frac{b_5}{\sqrt{a_4}}, \frac{b_6}{\sqrt{a_4}} \right]. \end{aligned} \quad (12)$$

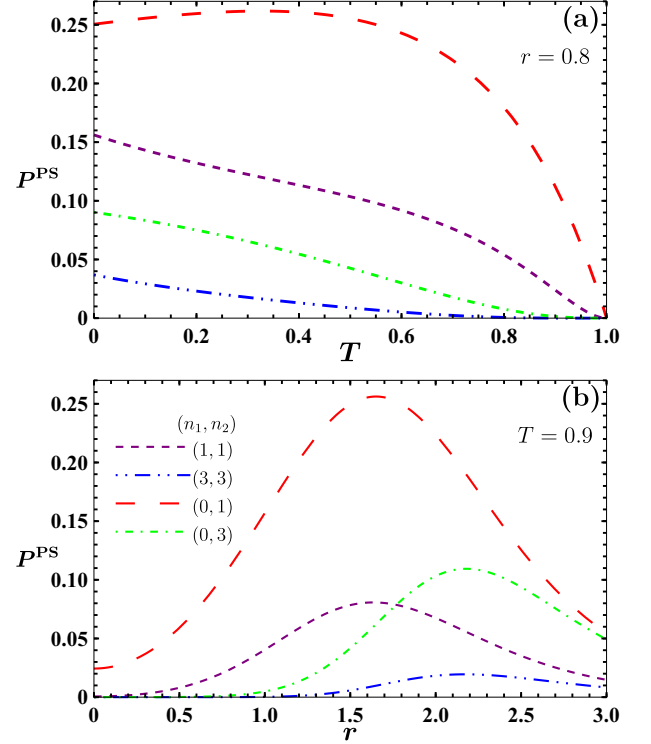


FIG. 2. Success probability P^{PS} of PSTMSC states as a function of (a) transmissivity T and (b) squeezing parameter r . The displacement has been taken as $d = 0.5$. (n_1, n_2) represents the number of photons subtracted from each mode.

We now analyze the success probability for various PSTMSC states as a function of transmissivity and squeezing parameter in Fig. 2. For numerical analysis, we have assumed $T_1 = T_2 = T$ throughout this paper. We see that the success probability decreases as transmissivity increases and approaches zero at unit transmissivity. The results show an optimum squeezing at which the probability is maximum. We notice that the Asym n -PSTMSC and Sym n -PSTMSC states achieve the maximum around the same squeezing; however, the magnitude of the success probability is less for Sym n -PSTMSC state as compared to Asym n -PSTMSC state. Furthermore, the success probability for Asym n -PSTMSC and Sym n -PSTMSC states decreases as n increases. We also noticed from our numerical analysis (not shown) that the maximum shifts to lower squeezing as the transmissivity decreases.

The normalized Wigner characteristic function $\chi_{A'_1 A'_2}^{\text{PS}}$

of the non-Gaussian PSTMSC state is obtained as

$$\chi_{A'_1 A'_2}^{\text{PS}}(\tau_1, \sigma_1, \tau_2, \sigma_2) = (P^{\text{PS}})^{-1} \tilde{\chi}_{A'_1 A'_2}^{\text{PS}}(\tau_1, \sigma_1, \tau_2, \sigma_2). \quad (13)$$

Several special cases can be obtained from the above expression. The Wigner characteristic function of the ideal PSTMSC state $\hat{a}_1^{n_1} \hat{a}_2^{n_2} |\text{TMSC}\rangle$ can be obtained by setting $T_1 = T_2 = 1$ in Eq. (13). Further, setting $d = 0$, and $T_1 = T_2 = 1$ in Eq. (13) yields the Wigner characteristic function of the ideal PSTMSV state $\hat{a}_1^{n_1} \hat{a}_2^{n_2} |\text{TMSV}\rangle$. Now we derive the Wigner characteristic function of PATMSC state.

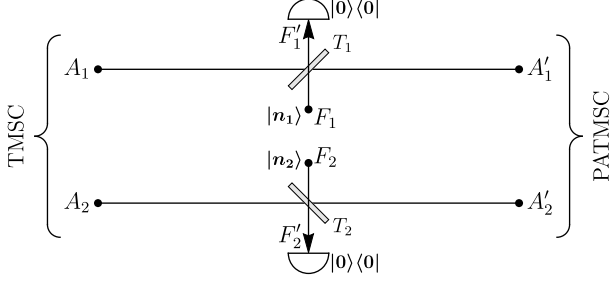


FIG. 3. Scheme for the preparation of PATMSC state. Modes A_1 and A_2 of TMSC state is mixed with modes F_1 and F_2 , initialized to Fock states $|n_1\rangle$ and $|n_2\rangle$, using beam splitter of transmissivity T_1 and T_2 , respectively. On-off detectors given by the POVM $\{|0\rangle\langle 0|, \mathbb{1} - |0\rangle\langle 0|\}$ and $\{|0\rangle\langle 0|, \mathbb{1} - |0\rangle\langle 0|\}$ are applied to modes F'_1 and F'_2 respectively. Simultaneous click of the ‘on’ elements of both the detectors represents successful addition of n_1 and n_2 photons to the TMSC state.

The schematic for the generation of PATMSC state is portrayed in Fig. 3. We mix the modes A_1 and A_2 of the TMSC state, with ancilla modes F_1 and F_2 , initiated to Fock states $|n_1\rangle$ and $|n_2\rangle$, using beam-splitters of transmissivity T_1 and T_2 respectively. The Wigner characteristic function of the four mode system post the beam splitter operations can be written as

$$\chi_{F_1 A_1 A_2 F_2}(\Lambda) = \chi_{A_1 A_2}(\Lambda_1, \Lambda_2) \chi_{|n_1\rangle}(\Lambda_3) \chi_{|n_2\rangle}(\Lambda_4). \quad (14)$$

The two beam splitters entangle the four modes. The Wigner characteristic function after the beam-splitter operations is given by

$$\chi_{F'_1 A'_1 A'_2 F'_2}(\Lambda) = \chi_{F_1 A_1 A_2 F_2}(B(T_1, T_2)^{-1} \Lambda). \quad (15)$$

The modes F'_1 and F'_2 are measured with on-off detectors represented by the POVM $\{\Pi_0 = |0\rangle\langle 0|, \mathbb{1} - \Pi_0\}$. When both the POVM elements Π_0 click simultaneously, n_1 and n_2 photons are considered to be added to the TMSC state. Analogous to the PS case, we consider symmetric PA for $n_1 = n_2 = n$ and asymmetric PA (on mode A_2) for $n_1 = 0, n_2 = n$ and $T_1 = 1$. The corresponding states are called Sym n -PATMSC and Asym n -PATMSC states. The unnormalized Wigner characteristic function for the

PATMSC state can be written as

$$\begin{aligned} \tilde{\chi}_{A'_1 A'_2}^{\text{PA}} &= \frac{1}{(2\pi)^2} \int d^2 \Lambda_3 d^2 \Lambda_4 \underbrace{\chi_{F'_1 A'_1 A'_2 F'_2}(\Lambda)}_{\text{Four mode entangled state}} \\ &\times \underbrace{\chi_{|0\rangle}(\Lambda_3)}_{\text{Projection on } |0\rangle\langle 0|} \underbrace{\chi_{|0\rangle}(\Lambda_4)}_{\text{Projection on } |0\rangle\langle 0|}. \end{aligned} \quad (16)$$

On integrating Eq. (16), we obtain

$$\begin{aligned} \tilde{\chi}_{A'_1 A'_2}^{\text{PA}} &= a_0 \exp(\mathbf{\Lambda}^T M_1 \mathbf{\Lambda} + \mathbf{\Lambda}^T M_2) \\ &\times \hat{\mathbf{F}}_1 \exp[-c_1 u_1 v_1 + c_2 u_1 + c_3 v_1 - c_4 u_2 v_2 \\ &+ c_5 u_2 + c_6 v_2 + c_7 (u_1 u_2 + v_1 v_2)], \end{aligned} \quad (17)$$

where the coefficients c_i are provided in Eq. (B9) of the Appendix B. The afore-derived expression can also be written in terms of two variable Hermite polynomial as

$$\begin{aligned} \tilde{\chi}_{A'_1 A'_2}^{\text{PA}} &= a_0 \frac{2^{-(n_1+n_2)}}{n_1! n_2!} \exp(\mathbf{\Lambda}^T M_1 \mathbf{\Lambda} + \mathbf{\Lambda}^T M_2) \\ &\times \sum_{i,j=0}^{\min(n_1, n_2)} \frac{c_1^{n_1}}{\sqrt{c_1}^{i+j}} \frac{c_4^{n_2}}{\sqrt{c_4}^{i+j}} \frac{c_7^{i+j}}{i! j!} P_i^{n_1} P_j^{n_2} P_i^{n_2} P_j^{n_1} \\ &\times H_{n_1-i, n_1-j} \left[\frac{c_2}{\sqrt{c_1}}, \frac{c_3}{\sqrt{c_1}} \right] H_{n_2-i, n_2-j} \left[\frac{c_5}{\sqrt{c_4}}, \frac{c_6}{\sqrt{c_4}} \right]. \end{aligned} \quad (18)$$

The probability of n_1 and n_2 photon addition on the TMSC state can be evaluated from the above equation (18) as follows:

$$\begin{aligned} P^{\text{PA}} &= \tilde{\chi}_{A'_1 A'_2}^{\text{PA}} \Big|_{\substack{\tau_1 = \sigma_1 = 0 \\ \tau_2 = \sigma_2 = 0}} = a_0 \hat{\mathbf{F}}_1 \exp[-c_1 u_1 v_1 + d_2 u_1 \\ &+ d_3 v_1 - c_4 u_2 v_2 + d_5 u_2 + d_6 v_2 + c_7 (u_1 u_2 + v_1 v_2)], \end{aligned} \quad (19)$$

where the coefficients d_i are given in Eq. (B10) of the Appendix B. Equation (19) can also be expressed in terms of two-variable Hermite polynomial:

$$\begin{aligned} P^{\text{PA}} &= a_0 \frac{2^{-(n_1+n_2)}}{n_1! n_2!} \sum_{i,j=0}^{\min(n_1, n_2)} \frac{c_1^{n_1}}{\sqrt{c_1}^{i+j}} \frac{c_4^{n_2}}{\sqrt{c_4}^{i+j}} \frac{c_7^{i+j}}{i! j!} P_i^{n_1} \\ &\times P_j^{n_2} P_i^{n_2} P_j^{n_1} H_{n_1-i, n_1-j} \left[\frac{d_2}{\sqrt{c_1}}, \frac{d_3}{\sqrt{c_1}} \right] H_{n_2-i, n_2-j} \left[\frac{d_5}{\sqrt{c_4}}, \frac{d_6}{\sqrt{c_4}} \right]. \end{aligned} \quad (20)$$

Now we analyze the success probability for the PATMSC states as a function of transmissivity and squeezing parameter in Fig. 4. Again we see that the success probability decreases as transmissivity increases and approaches zero at unit transmissivity. Further, the Asym n -PATMSC and Sym n -PATMSC states achieve a maximum around the same squeezing, and the magnitude of success probability for Sym n -PATMSC state is lower than the Asym n -PATMSC state. Further, the success probability for Asym n -PATMSC and Sym n -PATMSC states decrease as n increases. We also observed that the

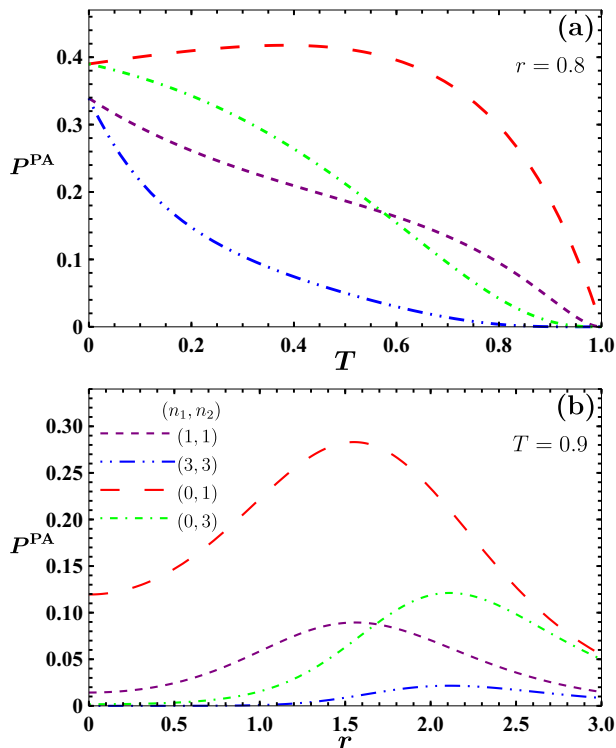


FIG. 4. Success probability P^{PA} of PATMSC states as a function of (a) transmissivity T and (b) squeezing parameter r . The displacement has been taken as $d = 0.5$. (n_1, n_2) represents the number of photons added to each mode.

maxima shifts to lower squeezing as the transmissivity decreases.

The normalized Wigner characteristic function $\chi_{A'_1 A'_2}^{\text{PA}}$ of the non-Gaussian PATMSC state is given by

$$\chi_{A'_1 A'_2}^{\text{PA}}(\tau_1, \sigma_1, \tau_2, \sigma_2) = (P^{\text{PA}})^{-1} \tilde{\chi}_{A'_1 A'_2}^{\text{PA}}(\tau_1, \sigma_1, \tau_2, \sigma_2). \quad (21)$$

We can obtain the Wigner characteristic function of several special cases from the above expression. For instance, by setting $T_1 = T_2 = 1$ in Eq. (21), we get the Wigner characteristic function of the ideal PATMSC state $\hat{a}_1^{\dagger m_1} \hat{a}_2^{\dagger m_2} |\text{TMSC}\rangle$. On further setting $d = 0$, we obtain the Wigner characteristic function of the ideal PATMSV state $\hat{a}_1^{\dagger m_1} \hat{a}_2^{\dagger m_2} |\text{TMSV}\rangle$.

III. CV QT USING PSTMSC AND PATMSC STATES

After deriving the Wigner characteristic function of the PSTMSC and PATMSC states, we derive the teleportation fidelity to teleport a coherent and squeezed vacuum state.

Here we consider the ideal Braunstein-Kimble (BK) protocol for the QT of an unknown input quantum state between two distant physical systems [1]. The schematic is shown in Fig. 5. In the protocol, Alice and Bob share

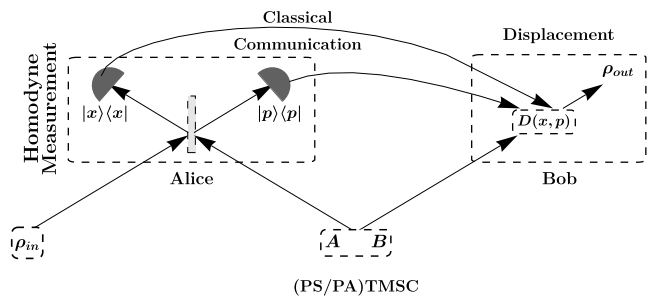


FIG. 5. Schematic of ideal Braunstein-Kimble protocol for the quantum teleportation of an unknown input quantum state. The shared resource state can be either TMSC, PSTMSC or PATMSC.

an entangled resource state. The density operator and the characteristic function of the entangled resource state is represented by $\rho_{A'_1 A'_2}$ and $\chi_{A'_1 A'_2}(\Lambda_1, \Lambda_2)$, respectively. Alice has the single mode input state that has to be teleported. We denote the density operator and the characteristic function of the unknown input state by ρ_{in} and $\chi_{\text{in}}(\Lambda_{\text{in}})$, respectively. Using a balanced beam splitter, Alice mixes her mode and the single mode input state. Alice then performs homodyne measurements of \hat{x} and \hat{p} quadratures on the two output modes of the beam splitter and classically communicates the result to Bob. Bob performs a displacement operation $D(x, p)$ on his mode, and consequently, the mode A'_2 with Bob is transformed to mode 'out'. The state corresponding to the mode 'out' is the teleported state. In the characteristic function formalism, we can write the teleported state as a product of the input state and the entangled resource state [40]:

$$\chi_{\text{out}}(\tau_2, \sigma_2) = \chi_{\text{in}}(\tau_2, \sigma_2) \chi_{A'_1 A'_2}(\tau_2, -\sigma_2, \tau_2, \sigma_2). \quad (22)$$

To assess the success of the QT protocol, we define fidelity of QT as the overlap between the single mode input state ρ_{in} and the output state ρ_{out} as $F = \text{Tr}[\rho_{\text{in}} \rho_{\text{out}}]$. The fidelity of QT in characteristic function can be written as [41]

$$F = \frac{1}{2\pi} \int d^2 \Lambda_2 \chi_{\text{in}}(\Lambda_2) \chi_{\text{out}}(-\Lambda_2). \quad (23)$$

The maximum fidelity of teleporting a coherent state without using a shared entangled state is $1/2$ [42, 43]; therefore, fidelity greater than $1/2$ signifies a success for CV QT. We note that perfect teleportation, *i.e.*, teleportation with unit fidelity, can only occur with an infinitely entangled resource state.

A. Teleportation of input coherent state

Now we evaluate the fidelity of teleportation for an input coherent state using entangled PSTMSC state (13) as a resource. The Wigner characteristic function for the coherent state is provided in Eq. (A21) of Appendix A. The

expression for fidelity can be evaluated using Eq. (23), which turns out to be

$$F^{\text{PS}} = \frac{e_0}{P^{\text{PS}}} \frac{2^{-(n_1+n_2)}}{n_1!n_2!} \sum_{i,j=0}^{\min(n_1,n_2)} \frac{e_1^{n_1}}{\sqrt{e_1}^{i+j}} \frac{e_4^{n_2}}{\sqrt{e_4}^{i+j}} \frac{e_7^{i+j}}{i!j!} P_i^{n_1} \times P_j^{n_1} P_i^{n_2} P_j^{n_2} H_{n_1-i, n_1-j} \left[\frac{e_2}{\sqrt{e_1}}, \frac{e_3}{\sqrt{e_1}} \right] H_{n_2-i, n_2-j} \left[\frac{e_5}{\sqrt{e_4}}, \frac{e_6}{\sqrt{e_4}} \right], \quad (24)$$

where the coefficients e_i are given in Eq. (B11) of the Appendix B. The afore-derived expression represents the fidelity of QT for a very general family of non-Gaussian resource states. By taking proper limits, we can obtain the fidelity of QT for various special cases as follows: (i) Ideal PS on TMSV state by setting $T_1 = T_2 = 1$. (ii) Realistic PS on TMSV state by setting $d = 0$. (iii) Ideal PS on TMSV state by setting $d = 0$ and $T_1 = T_2 = 1$. Further, we can obtain fidelity of QT for asymmetric PS operations (on mode A_2) by setting $n_1 = 0$ and $T_1 = 1$ in the aforementioned cases.

The fidelity of QT using TMSV resource state can be obtained by taking $n_1 = n_2 = 0$ and the $T_1 = T_2 = 1$ in Eq. (24):

$$F^{\text{TMSV}} = \frac{1+\lambda}{2} \exp[d^2(\lambda-1)], \quad \lambda = \tanh r. \quad (25)$$

Setting $d = 0$, we obtain the fidelity corresponding to the TMSV resource state: $(1+\lambda)/2$ [1]. Similarly, in the unit transmissivity limit with $n_1 = n_2 = 1$, the fidelity results matches with the resource state $\hat{a}_1\hat{a}_2|\text{TMSV}\rangle$ considered in Ref. [19]. We see that the fidelity is independent of displacement of the input coherent state and depends upon the displacement and squeezing of the TMSV state. Similarly, the fidelity of QT for an input coherent state using PATMSV resource state (21) can be evaluated using Eq. (23):

$$F^{\text{PA}} = \frac{e_0}{P^{\text{PA}}} \frac{2^{-(n_1+n_2)}}{n_1!n_2!} \sum_{i,j=0}^{\min(n_1,n_2)} \frac{f_1^{n_1}}{\sqrt{f_1}^{i+j}} \frac{f_4^{n_2}}{\sqrt{f_4}^{i+j}} \frac{f_7^{i+j}}{i!j!} P_i^{n_1} \times P_j^{n_1} P_i^{n_2} P_j^{n_2} H_{n_1-i, n_1-j} \left[\frac{f_2}{\sqrt{f_1}}, \frac{f_3}{\sqrt{f_1}} \right] H_{n_2-i, n_2-j} \left[\frac{f_5}{\sqrt{f_4}}, \frac{f_6}{\sqrt{f_4}} \right], \quad (26)$$

where the coefficients f_i are given in Eq. (B12) of the Appendix B. The fidelity results matches with the resource state $\hat{a}_1^\dagger\hat{a}_2^\dagger|\text{TMSV}\rangle$ obtained in the unit transmissivity limit with $n_1 = n_2 = 1$ [19].

We numerically analyze the fidelity of QT for an input coherent state as a function of transmissivity and squeezing for the PSTMSV resource state and plot these results in Fig. 6.

From Fig. 6(a), we observe that the fidelity of QT increases as transmissivity increases; however, as we noticed in Fig. 2(b) that the success probability approaches zero in the unit transmissivity limit. Therefore, we need to work in the $T < 1$ regime. For symmetric operations, the fidelity of QT is above 1/2 for all values of transmissivity for the considered squeezing parameter

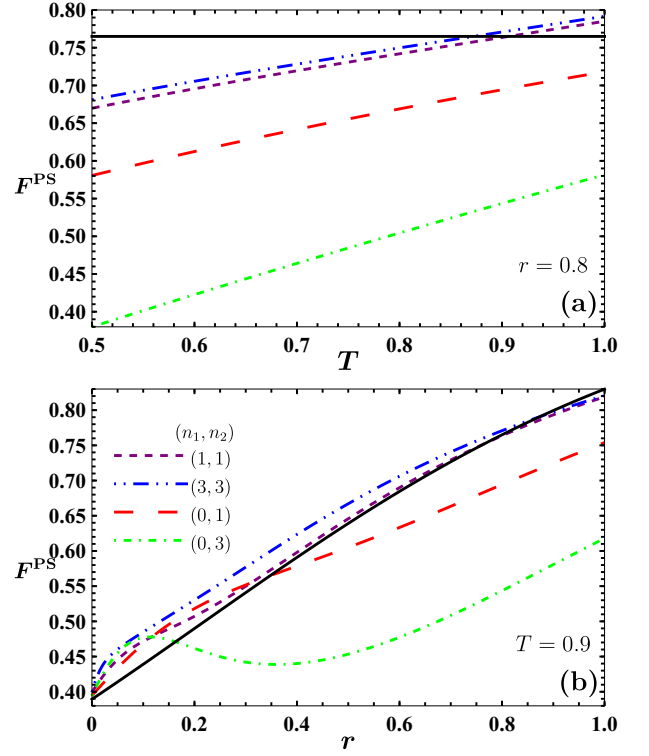


FIG. 6. Teleportation fidelity F^{PS} for an input coherent state using PSTMSV resource states as a function of (a) transmissivity T and (b) squeezing parameter r . The displacement has been taken as $d = 0.5$. The black solid curve represents the fidelity of teleportation for an input coherent state using the TMSV resource state.

$r = 0.8$. According to BK protocol, the excess value beyond the classical bound 1/2 is an indicator of the success of CV QT. While Asym 1-PSTMSV state surpasses the 1/2 limit for all transmissivity values, Asym 3-PSTMSV only surpasses the 1/2 limit for $T \approx 0.8$. Further, the teleportation fidelity for Sym 1-PSTMSV and Sym 3-PSTMSV states outperforms the TMSV state after a threshold transmissivity $T \approx 0.9$.

In Fig. 6(b), we see that Sym 1-PSTMSV and Sym 3-PSTMSV states outperform the TMSV state in the approximate interval $r \in (0, 0.8)$. Moreover, the teleportation fidelity for these states surpasses the classical limit 1/2 for $r \approx 0.15$, which is a positive result. Asym 1-PSTMSV state outperforms Sym 1-PSTMSV when the fidelity of teleportation is over the classical bound 1/2. However, Asym 3-PSTMSV state outperforms Sym 1-PSTMSV when the fidelity of teleportation is below the classical bound 1/2. Therefore this scenario does not reflect the success of the CV QT protocol.

The success probability for Sym 1-PSTMSV and Sym 3-PSTMSV states are of the order 10^{-2} and 10^{-5} at $r = 0.6$. For Asym 1-PSTMSV state the probability is of the order 10^{-2} at $r = 0.2$.

We study the teleportation fidelity of an input coherent state using the PATMSV resource state. Figure 7 shows

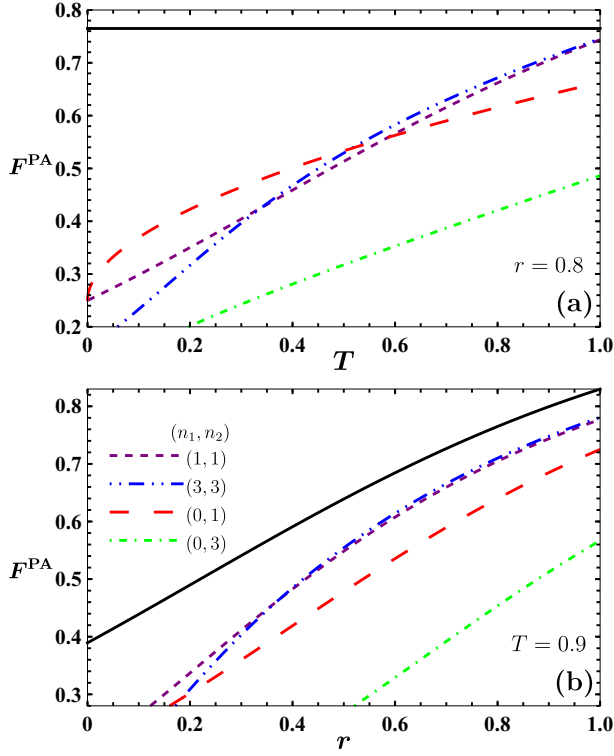


FIG. 7. Teleportation fidelity F^{PA} for an input coherent state using PATMSC resource states as a function of (a) transmissivity T and (b) squeezing parameter r . The displacement has been taken as $d = 0.5$. The black solid curve represents fidelity of teleportation for an input coherent state using the TMSC resource state.

the results. We observe that the symmetric and asymmetric photon addition only weakens the teleportation fidelity in the sense that PATMSC resource states underperform compared to the TMSC resource state. However, the PATMSC states do surpass the classical bound $1/2$, reflecting success for CV QT.

B. Teleportation of input squeezed vacuum state

We now consider the teleportation of input squeezed vacuum state with squeezing ϵ using entangled PSTMSC state as a resource state. The Wigner characteristic function of squeezed vacuum state can be obtained using Eq. (A22) of the Appendix A. The expression for the fidelity of QT can be evaluated using Eq. (23), which turns out to be

$$F^{\text{PS}} = \frac{\hat{\mathbf{F}}_1 \exp(\mathbf{u}^T M_3 \mathbf{u} + \mathbf{u}^T M_4 + m_0)}{P^{\text{PS}} \sqrt{b_0^2 + d_0^2 + 2b_0 d_0 \cosh(2\epsilon)}}, \quad (27)$$

where $d_0 = (\cosh r - \sinh r \sqrt{T_1 T_2})^2$ and the column vector \mathbf{u} is defined as $(u_1, v_1, u_2, v_2)^T$. Further the expressions for m_0 and the matrices M_3 and M_4 are provided in Eqs. (B13), (B14), and (B16) of the Appendix B.

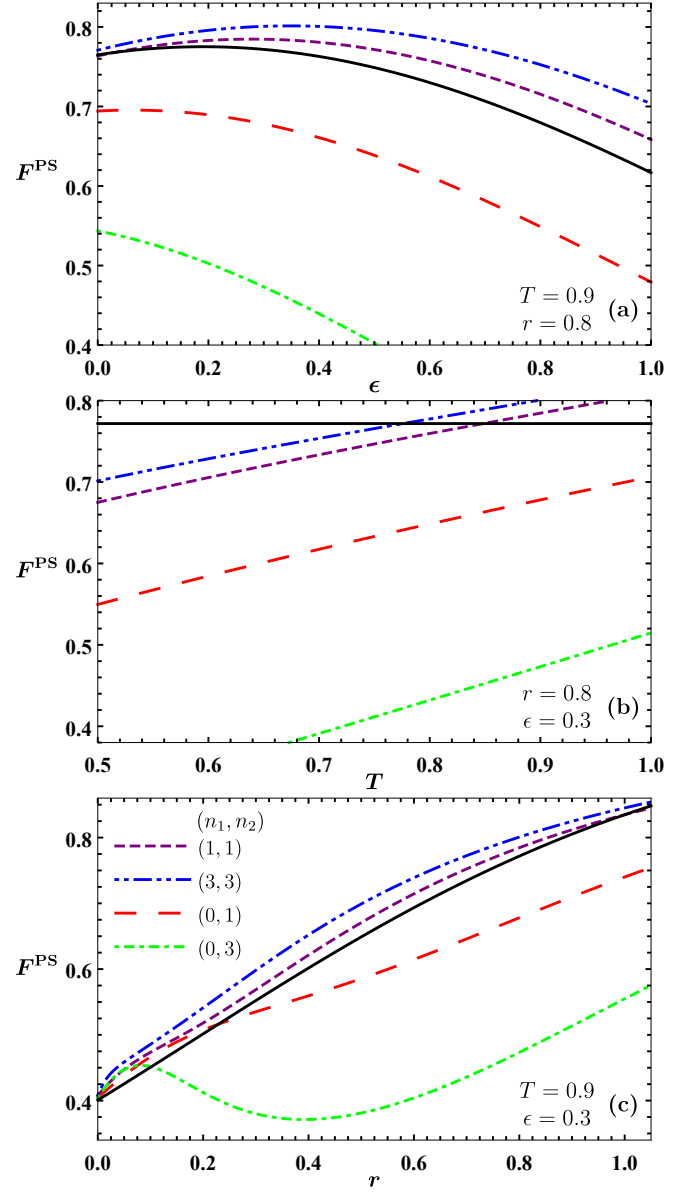


FIG. 8. (a) Teleportation fidelity F^{PS} for input squeezed vacuum state using PSTMSC resource states as a function of the squeezing parameter ϵ . (b) Teleportation fidelity F^{PS} for an input squeezed vacuum state using PSTMSC resource states as a function of transmissivity T . (c) Teleportation fidelity F^{PS} for an input squeezed vacuum state using PSTMSC resource states as a function of squeezing parameter r . The displacement has been taken as $d = 0.5$. The black solid curve represents fidelity of teleportation for an input squeezed vacuum state using the TMSC resource state.

On taking $n_1 = n_2 = 0$ and $T_1 = T_2 = 1$, we obtain fidelity of QT of an input squeezed vacuum state using

TMSC resource state:

$$F^{\text{TMSC}} = \left[\left(\frac{1 + \tanh(r + \epsilon)}{2} \right) \left(\frac{1 + \tanh(r - \epsilon)}{2} \right) \right]^{1/2} \times \exp [d^2 (\tanh(r + \epsilon) - 1)], \quad (28)$$

which depends on the squeezing ϵ of the input state and displacement and squeezing r of the TMSC state. Further on taking $\epsilon = 0$ in Eq. (28), we obtain Eq. (25), the fidelity of QT of an input coherent state using TMSC resource state.

We now proceed to evaluate the fidelity of QT of an input squeezed vacuum state using PATMSC resource state, which evaluates to

$$F^{\text{PA}} = \frac{\hat{\mathbf{F}}_1 \exp(\mathbf{u}^T M_5 \mathbf{u} + \mathbf{u}^T M_6 + m_0)}{P^{\text{PA}} \sqrt{b_0^2 + d_0^2 + 2b_0 d_0 \cosh(2\epsilon)}}, \quad (29)$$

where the explicit forms of the matrices M_5 and M_6 are provided in Eqs. (B18), and (B20) of the Appendix B.

We analyze the fidelity of QT of an input squeezed vacuum state using the PSTMSC resource state. We plot the teleportation fidelity as a function of the squeezing ϵ of the input squeezed vacuum state in Fig. 8(a). The fidelity of QT for the symmetric PSTMSC state and the TMSC state initially increases, attains a maximum value, and then starts to decrease as ϵ increases.

We plot the fidelity of QT as a function of transmissivity in Fig. 8(b). We observe that the performance of the symmetric PSTMSC state surpasses the TMSC state after a threshold transmissivity $T \approx 0.8$. The fidelity of QT as a function of squeezing parameter r is shown in Fig. 8(c). We observe that the qualitative behavior of the fidelity for different PSTMSC states is similar to that of Fig. 6, the teleportation fidelity for input coherent state.

In Fig. 9, we analyze the teleportation fidelity of input squeezed vacuum state using PATMSC resource state. We observe from Fig. 9(b) that the Sym 3-PATMSC state outperforms the TMSC state only for high value of transmissivity ($T \approx 0.99$). Further Fig. 9(c) shows that the Sym 3-PATMSC state outperforms the TMSC state for high squeezing parameter. We note that the success probability for Sym 3-PATMSC is of the order 10^{-8} at $r = 1$.

To conclude the analysis of fidelity of QT using PSTMSC and PATMSC resource states, we find that the symmetric PS is the most beneficial non-Gaussian operation. In Table I, we have provided the advantageous range of the squeezing parameter along with the success probability for non-Gaussian operations providing positive results.

TABLE I. Advantageous range of squeezing parameter and success probability.

Operation	Squeezing Range (coh)	Squeezing Range (sqv)	Success Probability
Asym 1-PS	$r \in [0.0, 0.4]$ for $T = 0.9$	$r \in [0.0, 0.2]$ for $T = 0.9$	$P \sim 10^{-2}$ at $r = 0.2$
Sym 1-PS	$r \in [0.0, 0.8]$ for $T = 0.9$	$r \in [0.0, 1.0]$ for $T = 0.9$	$P \sim 10^{-2}$ at $r = 0.6$
Sym 3-PS	$r \in [0.0, 0.8]$ for $T = 0.9$	$r \in [0.0, 1.1]$ for $T = 0.9$	$P \sim 10^{-5}$ at $r = 0.6$
Sym 3-PA	\emptyset for all values of T	$r \in [0.6, 2.0]$ for $T = 0.99$	$P \sim 10^{-8}$ at $r = 1$

IV. CONCLUSION

In this paper, we analytically derived the Wigner characteristic function for the families of PATMSC and PSTMSC states. Using the expression for the Wigner characteristic function, we computed the expression of the fidelity of quantum teleportation for input coherent states and squeezed vacuum states. For the PS case, our analysis showed that the symmetric PS operations turn out to be more advantageous compared to the asymmetric PS operations which was useful only in the low squeezing range. PA operations were in general, less useful than PS operations for quantum teleportation and it was only

the symmetric 3-PA which resulted in a modest improvement over the TMSC state for an input squeezed vacuum. We were able to recover the previous results available in this context as special cases from our more general analysis.

We considered an explicit physical model to carry out the PS and PA operations. As it turns out, the scheme succeeds only with a certain probability, leading to a reduction of available resources. The success probability for Sym 1-PS is of the order 10^{-2} , while for Sym 3-PS and Sym 3-PA, the orders drop to 10^{-5} and 10^{-8} , respectively. Therefore, for a realistic comparison we must take into account these success probabilities which further re-

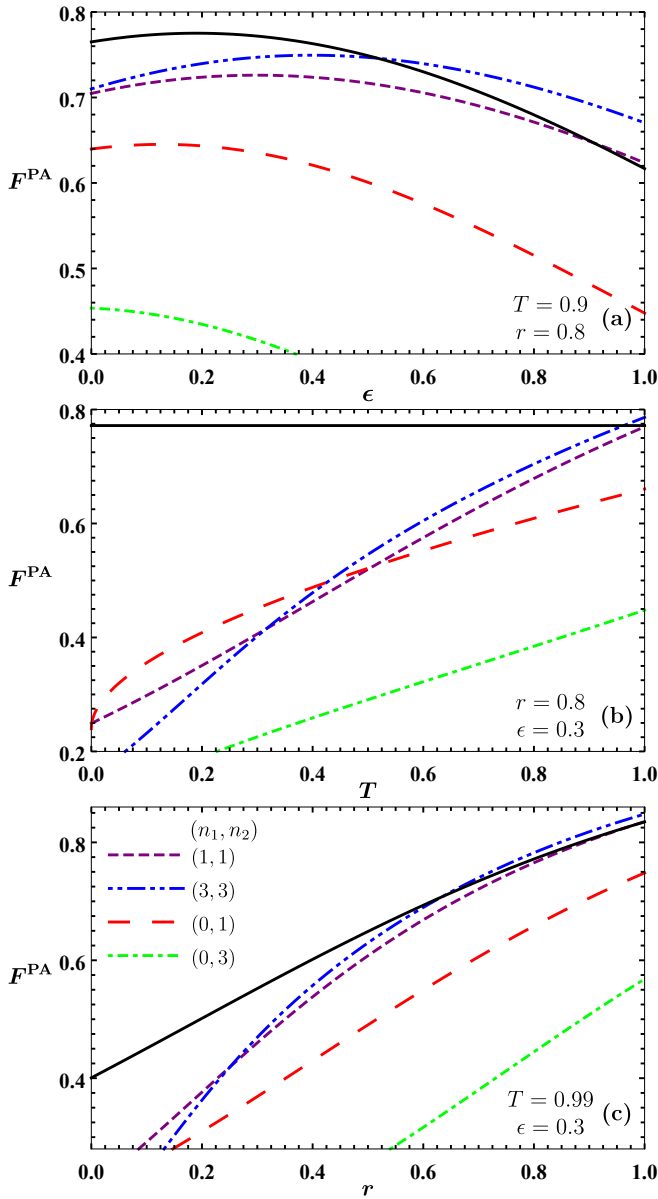


FIG. 9. (a) Teleportation fidelity F^{PA} for input squeezed vacuum state using PATMSC resource states as a function of the squeezing parameter ϵ . (b) Teleportation fidelity F^{PA} for an input squeezed vacuum state using PATMSC resource states as a function of transmissivity T . (c) Teleportation fidelity F^{PA} for an input squeezed vacuum state using PATMSC resource states as a function of squeezing parameter r . The displacement has been taken as $d = 0.5$. The black solid curve represents fidelity of teleportation for an input squeezed vacuum state using the TMSC resource state.

duces the reason for using these operations. In any case, given the overall picture, we conclude that the Sym 1-PS operation is the most profitable non-Gaussian operation for the purpose of carrying out quantum teleportation. We stress that a more efficient way of carrying out PS and PA operations is desirable if we want to use them for enhancement of the efficiency of QIP protocols based on

CV systems.

We expect that the current work, where we have explicitly computed the Wigner characteristic function for PSTMSC and PATMSC states will pave the way to better analyse the application of these non-Gaussian states in various other QIP protocols such as QKD, quantum metrology, and entanglement swapping.

ACKNOWLEDGEMENT

A and C.K. acknowledge the financial support from **DST/ICPS/QuST/Theme-1/2019/General** Project number Q-68.

Appendix A: Continuous variable systems, symplectic transformations and phase space description

We represent an n -mode continuous variable quantum system via n pairs of Hermitian quadrature operators \hat{q}_i, \hat{p}_i ($i = 1, \dots, n$) which can be grouped together in the form of a column vector as [44–48]

$$\hat{\xi} = (\hat{\xi}_i) = (\hat{q}_1, \hat{p}_1, \dots, \hat{q}_n, \hat{p}_n)^T, \quad i = 1, 2, \dots, 2n. \quad (\text{A1})$$

The bosonic commutation relation between them can be expressed in a compact form as ($\hbar=1$)

$$[\hat{\xi}_i, \hat{\xi}_j] = i\Omega_{ij}, \quad (i, j = 1, 2, \dots, 2n), \quad (\text{A2})$$

where Ω is the $2n \times 2n$ matrix given by

$$\Omega = \bigoplus_{k=1}^n \omega = \begin{pmatrix} \omega & & \\ & \ddots & \\ & & \omega \end{pmatrix}, \quad \omega = \begin{pmatrix} 0 & 1 \\ -1 & 0 \end{pmatrix}. \quad (\text{A3})$$

We can also represent an n -mode continuous variable quantum system via n -pairs of annihilation \hat{a}_i and creation operators \hat{a}_i^\dagger ($i = 1, 2, \dots, n$). The field annihilation and creation operators \hat{a}_i and \hat{a}_i^\dagger ($i = 1, 2, \dots, n$) can be expressed in terms of quadrature operators as

$$\hat{a}_i = \frac{1}{\sqrt{2}}(\hat{q}_i + i\hat{p}_i), \quad \hat{a}_i^\dagger = \frac{1}{\sqrt{2}}(\hat{q}_i - i\hat{p}_i). \quad (\text{A4})$$

Displacement operator : Displacement operator acting on the i^{th} mode is defined as

$$\hat{D}_i(a_i, b_i) = e^{i(b_i\hat{q}_i - a_i\hat{p}_i)}, \quad (\text{A5})$$

where a_i and b_i is the amount of displacement along \hat{q} and \hat{p} -quadrature of the i^{th} mode. Coherent state are generated by the action of the displacement operator on the vacuum state:

$$|a_i, b_i\rangle_i = \hat{D}_i(a_i, b_i)|0\rangle_i. \quad (\text{A6})$$

Symplectic transformations are linear homogeneous transformations, which are characterized by real $2n \times 2n$ matrices S and transform the quadrature operators as $\hat{\xi}_i \rightarrow \hat{\xi}'_i = S_{ij}\hat{\xi}_j$. The S matrices obey the canonical commutation relations (A2) leading to the condition $S\Omega S^T = \Omega$. These real transformations constitute a non-compact group in $2n$ dimensions known as symplectic group denoted by $Sp(2n, \mathcal{R})$. For each element $S \in Sp(2n, \mathcal{R})$, there exists an infinite dimensional unitary representation $\mathcal{U}(S)$ acting on the Hilbert space. Now we define three symplectic operations, which are relevant to this work [44, 47].

Single mode squeezing operation : The single mode squeezing operation transforms the quadrature operators $(\hat{q}, \hat{p})^T$ according to the symplectic matrix

$$S(r) = \begin{pmatrix} e^{-r} & 0 \\ 0 & e^r \end{pmatrix}. \quad (\text{A7})$$

The infinite dimensional unitary representation for the single mode squeezing operation can be written as

$$\mathcal{U}(S(r)) = \exp[r(a^2 - \hat{a}^\dagger^2)/2]. \quad (\text{A8})$$

Beam splitter operation : The two mode beam splitter operation is a symplectic transformation whose action on the quadrature operators $\hat{\xi} = (\hat{q}_i, \hat{p}_i, \hat{q}_j, \hat{p}_j)^T$ of a two mode system is given by

$$B_{ij}(T) = \begin{pmatrix} \sqrt{T} \mathbb{1}_2 & \sqrt{1-T} \mathbb{1}_2 \\ -\sqrt{1-T} \mathbb{1}_2 & \sqrt{T} \mathbb{1}_2 \end{pmatrix}, \quad (\text{A9})$$

where $\mathbb{1}_2$ is the 2×2 identity matrix. The infinite dimensional unitary representation corresponding to the beam splitter transformation is

$$\mathcal{U}(B_{ij}(T)) = \exp[\arccos(\sqrt{T})(\hat{a}_i^\dagger \hat{a}_j - \hat{a}_i \hat{a}_j^\dagger)]. \quad (\text{A10})$$

Two mode squeezing operation : The two mode squeezing operation is also a symplectic transformation whose action on the quadrature operators $(\hat{q}_i, \hat{p}_i, \hat{q}_j, \hat{p}_j)^T$ is given by

$$S_{ij}(r) = \begin{pmatrix} \cosh r \mathbb{1}_2 & \sinh r \mathbb{Z} \\ \sinh r \mathbb{Z} & \cosh r \mathbb{1}_2 \end{pmatrix}, \quad (\text{A11})$$

where $\mathbb{Z} = \text{diag}(1, -1)$. The corresponding infinite dimensional unitary operator acting on the Hilbert space is

$$\mathcal{U}(S_{ij}(r)) = \exp[r(\hat{a}_i^\dagger \hat{a}_j^\dagger - \hat{a}_i \hat{a}_j)]. \quad (\text{A12})$$

While the beam splitter operation acting on the Hilbert space through its infinite dimensional unitary representation $\mathcal{U}(B_{ij}(\theta))$ conserve the total photon number, single- and two-mode squeezing operator acting on the Hilbert space through its infinite dimensional unitary representation $\mathcal{U}(S_{ij}(r))$ do not conserve the total photon number. We note that all the infinite dimensional unitary transformations of the three aforementioned symplectic transformations are generated by quadratic Hamiltonians.

1. Phase space description

For our current work, it is convenient to work in phase space formalism, more specifically, Wigner characteristic function. For a density operator $\hat{\rho}$ of an n -mode quantum system, the corresponding Wigner characteristic function is given by

$$\chi(\Lambda) = \text{Tr}[\hat{\rho} \exp(-i\Lambda^T \Omega \hat{\xi})], \quad (\text{A13})$$

where $\xi = (\hat{q}_1, \hat{p}_1, \dots, \hat{q}_n, \hat{p}_n)^T$, $\Lambda = (\Lambda_1, \Lambda_2, \dots, \Lambda_n)^T$ with $\Lambda_i = (\tau_i, \sigma_i)^T \in \mathcal{R}^2$. The Wigner characteristic function for a single mode Fock state $|n\rangle$ can be evaluated using Eq. (A13) as

$$\chi_{|n\rangle}(\tau, \sigma) = \exp\left[-\frac{\tau^2}{4} - \frac{\sigma^2}{4}\right] L_n\left(\frac{\tau^2}{2} + \frac{\sigma^2}{2}\right), \quad (\text{A14})$$

where $L_n(x)$ is the Laguerre polynomial. It can further be expressed as

$$\chi_{|n\rangle}(\tau, \sigma) = \exp\left[-\frac{\tau^2}{4} - \frac{\sigma^2}{4}\right] \hat{F} e^{2st+s(\tau+i\sigma)-t(\tau-i\sigma)}, \quad (\text{A15})$$

with

$$\hat{F} = \frac{1}{2^n n!} \frac{\partial^n}{\partial s^n} \frac{\partial^n}{\partial t^n} \{\bullet\}_{s=t=0}. \quad (\text{A16})$$

For an n mode system, the first order moments are defined as

$$\mathbf{d} = \langle \hat{\xi} \rangle = \text{Tr}[\hat{\rho} \hat{\xi}], \quad (\text{A17})$$

and the second order moments, which can be written in the form of a real symmetric $2n \times 2n$ matrix, is defined as

$$V = (V_{ij}) = \frac{1}{2} \langle \{\Delta \hat{\xi}_i, \Delta \hat{\xi}_j\} \rangle, \quad (\text{A18})$$

where $\Delta \hat{\xi}_i = \hat{\xi}_i - \langle \hat{\xi}_i \rangle$, and $\{ \cdot, \cdot \}$ denotes anti-commutator. This matrix is called covariance matrix. The uncertainty principle puts the following condition on the covariance matrix:

$$V + \frac{i}{2} \Omega \geq 0. \quad (\text{A19})$$

A state is called a Gaussian state if the corresponding Wigner characteristic function is a Gaussian. Gaussian states are completely determined by their first and second order moments. For a Gaussian state, the Wigner characteristic function is given by [47, 49]

$$\chi(\Lambda) = \exp\left[-\frac{1}{2} \Lambda^T (\Omega V \Omega^T) \Lambda - i(\Omega \mathbf{d})^T \Lambda\right], \quad (\text{A20})$$

where V is the covariance matrix of the state and \mathbf{d} represents the displacement of the Gaussian state. Using

the above expression, the Wigner characteristic function of a single mode coherent state with displacement $\mathbf{d} = (d_x, d_p)^T$ turns out to be

$$\chi_{\text{coh}}(\Lambda) = \exp \left[-\frac{1}{4}(\tau^2 + \sigma^2) - i(\tau d_p - \sigma d_x) \right]. \quad (\text{A21})$$

Similarly, the characteristic function of a single mode squeezed vacuum state obtained by the action of a single mode squeezing operator (A8) on vacuum state evaluates to

$$\chi_{\text{sqv}}(\Lambda) = \exp \left[-\frac{1}{4}(\tau^2 e^{2r} + \sigma^2 e^{-2r}) \right]. \quad (\text{A22})$$

For a homogeneous symplectic transformation S and its infinite dimensional unitary representation $\mathcal{U}(S)$, the density operator transforms as $\rho \rightarrow \mathcal{U}(S)\rho\mathcal{U}(S)^\dagger$. The corresponding transformation of the displacement vector, covariance matrix and Wigner characteristic function is given by [44, 47, 49]

$$\mathbf{d} \rightarrow S\mathbf{d}, \quad V \rightarrow SVS^T, \quad \text{and } \chi(\Lambda) \rightarrow \chi(S^{-1}\Lambda). \quad (\text{A23})$$

We conclude this brief introduction of CV systems and its phase space formalism with a note that most of the concepts discussed are available at length in Refs. [44, 47, 48].

Appendix B: Matrices and coefficients appearing in the Wigner characteristic function, success probability and the fidelity of QT using PSTMSC and PATMSC state.

1. Wigner characteristic function and probability expression of the PSTMSC state

Here we provide the values of a_i and b_i , which appear in the Wigner characteristic function (10) and probability expression (11) of the PSTMSC state. The values for coefficients a_i and b_i are given by

$$\begin{aligned} a_0 &= b_0^{-1} \exp \left(d^2 \left(\frac{t_1^2 + t_2^2}{b_0} - 2 \right) \right), \\ a_1 &= -b_0^{-1} (\alpha^2 r_1^2 t_2^2), \\ a_2 &= b_2 - \frac{r_1 t_2 \alpha}{b_0} (\alpha t_1 t_2 (\tau_1 + i\sigma_1) + i\beta (i\tau_2 + \sigma_2)), \\ a_3 &= b_3 + \frac{r_1 t_2 \alpha}{b_0} (\alpha t_1 t_2 (\tau_1 - i\sigma_1) - \beta (\tau_2 + i\sigma_2)), \\ a_4 &= -b_0^{-1} (\alpha^2 r_2^2 t_1^2), \\ a_5 &= b_5 - \frac{r_2 t_1 \alpha}{b_0} (\alpha t_1 t_2 (\tau_2 + i\sigma_2) + i\beta (i\tau_1 + \sigma_1)), \\ a_6 &= b_6 + \frac{r_2 t_1 \alpha}{b_0} (\alpha t_1 t_2 (\tau_2 - i\sigma_2) - \beta (\tau_1 + i\sigma_1)), \\ a_7 &= b_0^{-1} (\alpha \beta r_1 r_2), \end{aligned} \quad (\text{B1})$$

where,

$$\begin{aligned} b_0 &= 1 + \alpha^2 (1 - t_1^2 t_2^2), \\ b_2 &= \frac{r_1 d}{b_0} (i+1) (i\alpha t_2^2 - \beta), \\ b_3 &= \frac{r_1 d}{b_0} (i+1) (i\beta - \alpha t_2^2), \\ b_5 &= \frac{r_2 d}{b_0} (i+1) (i\alpha t_1^2 - \beta), \\ b_6 &= \frac{r_2 d}{b_0} (i+1) (i\beta - \alpha t_1^2). \end{aligned} \quad (\text{B2})$$

Here $t_i = \sqrt{T_i}$ and $r_i = \sqrt{1 - T_i}$ ($i = 1, 2$). Further $\alpha = \sinh r$ and $\beta = \cosh r$. The matrix M_1 is given by

$$M_1 = \frac{-1}{4b_0} \begin{pmatrix} c_0 & 0 & -2\alpha\beta t_1 t_2 & 0 \\ 0 & c_0 & 0 & 2\alpha\beta t_1 t_2 \\ -2\alpha\beta t_1 t_2 & 0 & c_0 & 0 \\ 0 & 2\alpha\beta t_1 t_2 & 0 & c_0 \end{pmatrix}, \quad (\text{B3})$$

where $c_0 = 1 + \alpha^2 (1 + t_1^2 t_2^2)$. The explicit form of matrix M_2 can be written as

$$M_2 = \frac{d}{ib_0} \begin{pmatrix} t_1 (\beta - \alpha t_2^2) \\ -t_1 (\beta + \alpha t_2^2) \\ t_2 (\beta - \alpha t_1^2) \\ -t_2 (\beta + \alpha t_1^2) \end{pmatrix}. \quad (\text{B4})$$

Expressing Eq. (8) in terms of two variable Hermite polynomials

We first provide two identities concerning two variable Hermite polynomials and its differentiation:

$$\begin{aligned} H_{m,n}(x, y) &= \sum_{i=0}^{\min(m,n)} \frac{(-1)^i m! n! x^{m-i} y^{n-i}}{i! (m-i)! (n-i)!} \\ &= \frac{\partial^m}{\partial s^m} \frac{\partial^n}{\partial t^n} \exp(-st + sx + ty) \Big|_{s=t=0}. \end{aligned} \quad (\text{B5})$$

and

$$\frac{\partial^i}{\partial x^i} \frac{\partial^j}{\partial y^j} H_{m,n}(x, y) = \frac{m! n!}{(m-i)! (n-j)!} H_{m-i, n-j}(x, y), \quad (\text{B6})$$

Now we consider the part of Eq. (8) that depends only on u_i and v_i ($i = 1, 2$) and arrange them as follows:

$$\begin{aligned}
& \widehat{\mathbf{F}}_1 e^{a_7(u_1 u_2 + v_1 v_2)} e^{-a_1 u_1 v_1 + a_2 u_1 + a_3 v_1} e^{-a_4 u_2 v_2 + a_5 u_2 + a_6 v_2} \\
&= \widehat{\mathbf{F}}_1 \sum_{i=0}^{\infty} \frac{(a_7 u_1 u_2)^i}{i!} \sum_{j=0}^{\infty} \frac{(a_7 v_1 v_2)^j}{j!} e^{-a_1 u_1 v_1 + a_2 u_1 + a_3 v_1} \\
&\quad \times e^{-a_4 u_2 v_2 + a_5 u_2 + a_6 v_2} \\
&= \widehat{\mathbf{F}}_1 \sum_{i=0}^{\infty} \frac{(a_7)^i}{i!} \sum_{j=0}^{\infty} \frac{(a_7)^j}{j!} \partial_{a_2}^i \partial_{a_5}^i \partial_{a_3}^j \partial_{a_6}^j e^{-a_1 u_1 v_1 + a_2 u_1 + a_3 v_1} \\
&\quad \times e^{-a_4 u_2 v_2 + a_5 u_2 + a_6 v_2} \\
&= \sum_{i,j=0}^{\infty} \frac{(a_7)^{i+j}}{i! j!} \partial_{a_2}^i \partial_{a_5}^i \partial_{a_3}^j \partial_{a_6}^j a_1^{n_1} H_{n_1, n_1} \left[\frac{a_2}{\sqrt{a_1}}, \frac{a_3}{\sqrt{a_1}} \right] \\
&\quad \times a_4^{n_2} H_{n_2, n_2} \left[\frac{a_5}{\sqrt{a_4}}, \frac{a_6}{\sqrt{a_4}} \right]. \tag{B7}
\end{aligned}$$

Now we use Eq.(B7) to obtain the final form (10):

$$\begin{aligned}
& \sum_{i,j=0}^{\min(n_1, n_2)} \frac{(a_7)^{i+j}}{i! j!} a_1^{n_1} \frac{P_i^{n_1} P_j^{n_1}}{\sqrt{a_1}^{i+j}} H_{n_1-i, n_1-j} \left[\frac{a_2}{\sqrt{a_1}}, \frac{a_3}{\sqrt{a_1}} \right] \\
&\quad \times a_4^{n_2} \frac{P_i^{n_2} P_j^{n_2}}{\sqrt{a_4}^{i+j}} H_{n_2-i, n_2-j} \left[\frac{a_5}{\sqrt{a_4}}, \frac{a_6}{\sqrt{a_4}} \right]. \tag{B8}
\end{aligned}$$

2. Wigner characteristic function and probability expression of the PATMSC state

Now we furnish the values of the coefficients c_i and d_i arising in the Wigner characteristic function (17) and probability expression (19) of the PATMSC state. The values for coefficients c_i and d_i are given as follows:

$$\begin{aligned}
c_1 &= -b_0^{-1}(\beta^2 r_1^2), \\
c_2 &= d_2 - \frac{r_1 \beta}{b_0}(\alpha t_1 t_2 (\tau_2 - i\sigma_2) - \beta(\tau_1 + i\sigma_1)) \\
c_3 &= d_3 + \frac{r_1 \beta}{b_0}(\alpha t_1 t_2 (\tau_2 + i\sigma_2) + i\beta(i\tau_1 + \sigma_1)) \\
c_4 &= -b_0^{-1}(\beta^2 r_2^2) \\
c_5 &= d_5 - \frac{r_2 \beta}{b_0}(\alpha t_1 t_2 (\tau_1 - i\sigma_1) - \beta(\tau_2 + i\sigma_2)) \\
c_6 &= d_6 + \frac{r_2 \beta}{b_0}(\alpha t_1 t_2 (\tau_1 + i\sigma_1) + i\beta(i\tau_2 + \sigma_2)) \\
c_7 &= b_0^{-1}(\alpha \beta r_1 r_2 t_1 t_2)
\end{aligned} \tag{B9}$$

where,

$$\begin{aligned}
d_2 &= -t_1 b_2, & d_5 &= -t_2 b_5, \\
d_3 &= -t_1 b_3, & d_6 &= -t_2 b_6.
\end{aligned} \tag{B10}$$

3. Fidelity for input coherent state using PSTMSC and PATMSC state

The coefficients e_i appearing in the fidelity of QT of input coherent state using PSTMSC state (24) are

$$\begin{aligned}
e_0 &= (b_0 + d_0)^{-1} \exp \left(d^2 \left(\frac{t_1^2 + t_2^2}{b_0 + d_0} - 2 \right) \right), \\
e_1 &= -(b_0 + d_0)^{-1} (\alpha^2 r_1^2 t_2^2), \\
e_2 &= \frac{r_1 d}{b_0 + d_0} (i+1) (\alpha t_2 (t_1 + i t_2) - 2\beta), \\
e_3 &= \frac{r_1 d}{b_0 + d_0} (i+1) (2i\beta - \alpha t_2 (i t_1 + t_2)), \\
e_4 &= -(b_0 + d_0)^{-1} (\alpha^2 r_2^2 t_1^2), \\
e_5 &= \frac{r_2 d}{b_0 + d_0} (i+1) (\alpha t_1 (i t_1 + t_2) - 2\beta), \\
e_6 &= \frac{r_2 d}{b_0 + d_0} (i+1) (2i\beta - \alpha t_1 (t_1 + i t_2)), \\
e_7 &= (b_0 + d_0)^{-1} \alpha r_1 r_2 (2\beta - \alpha t_1 t_2),
\end{aligned} \tag{B11}$$

where $d_0 = (\beta - \alpha t_1 t_2)^2$. Further, the coefficients f_i arising in the fidelity of QT of input coherent state using PATMSC state (26) are given by

$$\begin{aligned}
f_1 &= -(b_0 + d_0)^{-1} (\beta^2 r_1^2), \\
f_2 &= \frac{r_1 d \beta}{b_0 + d_0} (i+1) (t_1 - i t_2), \\
f_3 &= \frac{r_1 d \beta}{b_0 + d_0} (i+1) (t_2 - i t_1), \\
f_4 &= -(b_0 + d_0)^{-1} (\beta^2 r_2^2), \\
f_5 &= \frac{r_2 d \beta}{b_0 + d_0} (i+1) (t_2 - i t_1), \\
f_6 &= \frac{r_2 d \beta}{b_0 + d_0} (i+1) (t_1 - i t_2), \\
f_7 &= (b_0 + d_0)^{-1} (\beta^2 r_1 r_2).
\end{aligned} \tag{B12}$$

4. Fidelity for input squeezed vacuum state using PSTMSC and PATMSC state

The expression for m_0 in the fidelity of QT of input squeezed vacuum state using PSTMSC state (27) is

$$m_0 = d^2 \left(\frac{(t_1^2 + t_2^2) \delta + 2t_1 t_2 \gamma + b_0 (t_1^2 + t_2^2) d_0^{-1}}{2(c_0 + b_0 \delta)} - 2 \right), \tag{B13}$$

with $\gamma = \sinh(2\epsilon)$, and $\delta = \cosh(2\epsilon)$. The matrix M_3 is given by

$$M_3 = \frac{1}{2(c_0 + b_0 \delta)} \begin{pmatrix} g_1 & g_2 & g_3 & g_4 \\ g_2 & g_1 & g_4 & g_3 \\ g_3 & g_4 & g_5 & g_6 \\ g_4 & g_3 & g_6 & g_5 \end{pmatrix}, \tag{B14}$$

where

$$\begin{aligned}
g_1 &= -\alpha^2 r_1^2 t_2^2 \gamma, \\
g_2 &= \alpha^2 r_1^2 t_2^2 \left(\frac{b_0}{d_0} + \delta \right), \\
g_3 &= \alpha r_1 r_2 \left(\frac{c_0}{\sqrt{d_0}} + \beta + \delta \left(\frac{b_0}{\sqrt{d_0}} + \beta \right) \right), \\
g_4 &= 2\alpha^2 r_1 r_2 t_1 t_2 \gamma, \\
g_5 &= -\alpha^2 r_2^2 t_1^2 \gamma, \\
g_6 &= \alpha^2 r_2^2 t_1^2 \left(\frac{b_0}{d_0} + \delta \right).
\end{aligned} \tag{B15}$$

The matrix M_4 is given by

$$M_4 = \frac{d(i+1)}{2(c_0 + b_0\delta)} \begin{pmatrix} \alpha r_1 t_2 (t_1 - it_2) g_7 + g_8 \\ \alpha r_1 t_2 (t_2 - it_1) g_9 - ig_8 \\ \alpha r_2 t_1 (t_2 - it_1) g_7 + g_{10} \\ \alpha r_2 t_1 (t_1 - it_2) g_9 - ig_{10} \end{pmatrix}, \tag{B16}$$

where

$$\begin{aligned}
g_7 &= \frac{b_0}{d_0} + \delta - i\gamma, & g_9 &= \frac{b_0}{d_0} + \delta + i\gamma, \\
g_8 &= 2\beta r_1 (1 + \delta), & g_{10} &= 2\beta r_2 (1 + \delta).
\end{aligned} \tag{B17}$$

The expression for M_5 in the fidelity of QT of input squeezed vacuum state using PATMSC state (29) is

$$M_5 = \frac{1}{2(c_0 + b_0\delta)} \begin{pmatrix} h_1 & h_2 & h_3 & h_4 \\ h_2 & h_1 & h_4 & h_3 \\ h_3 & h_4 & h_5 & h_6 \\ h_4 & h_3 & h_6 & h_5 \end{pmatrix}, \tag{B18}$$

where,

$$\begin{aligned}
h_1 &= -\beta^2 r_1^2 \gamma, \\
h_2 &= \beta^2 r_1^2 \left(\frac{b_0}{d_0} + \delta \right), \\
h_3 &= \beta r_1 r_2 \left(\frac{c_0}{\sqrt{d_0}} - \alpha t_1 t_2 + \delta \left(\frac{b_0}{\sqrt{d_0}} + \alpha t_1 t_2 \right) \right) \\
h_4 &= \beta^2 r_1 r_2 \gamma, \\
h_5 &= -\beta^2 r_2^2 \gamma, \\
h_6 &= \beta^2 r_2^2 \left(\frac{b_0}{d_0} + \delta \right).
\end{aligned} \tag{B19}$$

The matrix M_6 is given by

$$M_6 = \frac{d(i+1)}{2(c_0 + b_0\delta)} \begin{pmatrix} r_1(t_1 h_7 - it_2 h_8 + \beta\gamma(t_2 + it_1)) \\ r_1(t_2 h_8 - it_1 h_7 - \beta\gamma(t_1 + it_2)) \\ r_2(t_2 h_7 - it_1 h_8 + \beta\gamma(t_1 + it_2)) \\ r_2(t_1 h_8 - it_2 h_7 - \beta\gamma(t_2 + it_1)) \end{pmatrix}, \tag{B20}$$

where

$$\begin{aligned}
h_7 &= \beta \left(\frac{b_0}{d_0} + \delta \right), \text{ and} \\
h_8 &= \alpha t_1 t_2 \left(\frac{b_0}{d_0} + \delta \right) + b_0 \left(\frac{d_0}{b_0} + \delta \right) d_0^{-1/2}.
\end{aligned} \tag{B21}$$

-
- [1] S. L. Braunstein and H. J. Kimble, Teleportation of continuous quantum variables, *Phys. Rev. Lett.* **80**, 869 (1998).
- [2] P. van Loock and S. L. Braunstein, Unconditional teleportation of continuous-variable entanglement, *Phys. Rev. A* **61**, 010302 (1999).
- [3] F. Laudenbach, C. Pacher, C.-H. F. Fung, A. Poppe, M. Peev, B. Schrenk, M. Hentschel, P. Walther, and H. Hübel, Continuous-variable quantum key distribution with gaussian modulation—the theory of practical implementations, *Advanced Quantum Technologies* **1**, 1800011 (2018).
- [4] M. Walschaers, Non-gaussian quantum states and where to find them, *PRX Quantum* **2**, 030204 (2021).
- [5] G. S. Agarwal and K. Tara, Nonclassical properties of

- states generated by the excitations on a coherent state, *Phys. Rev. A* **43**, 492 (1991).
- [6] A. Kitagawa, M. Takeoka, M. Sasaki, and A. Chefles, Entanglement evaluation of non-gaussian states generated by photon subtraction from squeezed states, *Phys. Rev. A* **73**, 042310 (2006).
- [7] A. Ourjoumteev, A. Dantan, R. Tualle-Brouiri, and P. Grangier, Increasing entanglement between gaussian states by coherent photon subtraction, *Phys. Rev. Lett.* **98**, 030502 (2007).
- [8] H. Takahashi, J. S. Neergaard-Nielsen, M. Takeuchi, M. Takeoka, K. Hayasaka, A. Furusawa, and M. Sasaki, Entanglement distillation from gaussian input states, *Nature Photonics* **4**, 178 (2010).
- [9] S. L. Zhang and P. van Loock, Distillation of mixed-state

- continuous-variable entanglement by photon subtraction, *Phys. Rev. A* **82**, 062316 (2010).
- [10] C. Navarrete-Benlloch, R. García-Patrón, J. H. Shapiro, and N. J. Cerf, Enhancing quantum entanglement by photon addition and subtraction, *Phys. Rev. A* **86**, 012328 (2012).
- [11] S.-H. Tan, B. I. Erkmen, V. Giovannetti, S. Guha, S. Lloyd, L. Maccone, S. Pirandola, and J. H. Shapiro, Quantum illumination with gaussian states, *Phys. Rev. Lett.* **101**, 253601 (2008).
- [12] E. D. Lopaeva, I. Ruo Berchera, I. P. Degiovanni, S. Olivares, G. Brida, and M. Genovese, Experimental realization of quantum illumination, *Phys. Rev. Lett.* **110**, 153603 (2013).
- [13] S. Zhang, J. Guo, W. Bao, J. Shi, C. Jin, X. Zou, and G. Guo, Quantum illumination with photon-subtracted continuous-variable entanglement, *Phys. Rev. A* **89**, 062309 (2014).
- [14] L. Fan and M. S. Zubairy, Quantum illumination using non-gaussian states generated by photon subtraction and photon addition, *Phys. Rev. A* **98**, 012319 (2018).
- [15] R. Gupta, S. Roy, T. Das, and A. Sen(De), Quantum illumination with noisy probes: Conditional advantages of non-gaussianity, *Physics Letters A* **505**, 129446 (2024).
- [16] T. Opatrný, G. Kurizki, and D.-G. Welsch, Improvement on teleportation of continuous variables by photon subtraction via conditional measurement, *Phys. Rev. A* **61**, 032302 (2000).
- [17] A. Kitagawa, M. Takeoka, M. Sasaki, and A. Chefles, Entanglement evaluation of non-gaussian states generated by photon subtraction from squeezed states, *Phys. Rev. A* **73**, 042310 (2006).
- [18] F. Dell'Anno, S. De Siena, L. Albano, and F. Illuminati, Continuous-variable quantum teleportation with non-gaussian resources, *Phys. Rev. A* **76**, 022301 (2007).
- [19] Y. Yang and F.-L. Li, Entanglement properties of non-gaussian resources generated via photon subtraction and addition and continuous-variable quantum-teleportation improvement, *Phys. Rev. A* **80**, 022315 (2009).
- [20] S. Wang, L.-L. Hou, X.-F. Chen, and X.-F. Xu, Continuous-variable quantum teleportation with non-gaussian entangled states generated via multiple-photon subtraction and addition, *Phys. Rev. A* **91**, 063832 (2015).
- [21] X.-x. Xu, Enhancing quantum entanglement and quantum teleportation for two-mode squeezed vacuum state by local quantum-optical catalysis, *Phys. Rev. A* **92**, 012318 (2015).
- [22] L. Hu, Z. Liao, and M. S. Zubairy, Continuous-variable entanglement via multiphoton catalysis, *Phys. Rev. A* **95**, 012310 (2017).
- [23] A. Patra, R. Gupta, S. Roy, and A. Sen(De), Significance of fidelity deviation in continuous-variable teleportation, *Phys. Rev. A* **106**, 022433 (2022).
- [24] C. Kumar and S. Arora, Success probability and performance optimization in non-gaussian continuous-variable quantum teleportation, *Phys. Rev. A* **107**, 012418 (2023).
- [25] C. Kumar, M. Sharma, and S. Arora, Continuous variable quantum teleportation in a dissipative environment: Comparison of non-gaussian operations before and after noisy channel, *Advanced Quantum Technologies* **7**, 2300344 (2024).
- [26] R. Birrittella, J. Mimih, and C. C. Gerry, Multiphoton quantum interference at a beam splitter and the approach to heisenberg-limited interferometry, *Phys. Rev. A* **86**, 063828 (2012).
- [27] R. Carranza and C. C. Gerry, Photon-subtracted two-mode squeezed vacuum states and applications to quantum optical interferometry, *J. Opt. Soc. Am. B* **29**, 2581 (2012).
- [28] D. Braun, P. Jian, O. Pinel, and N. Treps, Precision measurements with photon-subtracted or photon-added gaussian states, *Phys. Rev. A* **90**, 013821 (2014).
- [29] Y. Ouyang, S. Wang, and L. Zhang, Quantum optical interferometry via the photon-added two-mode squeezed vacuum states, *J. Opt. Soc. Am. B* **33**, 1373 (2016).
- [30] H. Zhang, W. Ye, C. Wei, Y. Xia, S. Chang, Z. Liao, and L. Hu, Improved phase sensitivity in a quantum optical interferometer based on multiphoton catalytic two-mode squeezed vacuum states, *Phys. Rev. A* **103**, 013705 (2021).
- [31] C. Kumar, Rishabh, and S. Arora, Realistic non-gaussian-operation scheme in parity-detection-based mach-zehnder quantum interferometry, *Phys. Rev. A* **105**, 052437 (2022).
- [32] C. Kumar, Rishabh, M. Sharma, and S. Arora, Parity-detection-based mach-zehnder interferometry with coherent and non-gaussian squeezed vacuum states as inputs, *Phys. Rev. A* **108**, 012605 (2023).
- [33] C. Kumar, Rishabh, and S. Arora, Enhanced phase estimation in parity-detection-based mach-zehnder interferometer using non-gaussian two-mode squeezed thermal input state, *Annalen der Physik* **535**, 2300117 (2023).
- [34] H. Nha and H. J. Carmichael, Proposed test of quantum nonlocality for continuous variables, *Phys. Rev. Lett.* **93**, 020401 (2004).
- [35] R. García-Patrón, J. Fiurásek, N. J. Cerf, J. Wenger, R. Tualle-Brouri, and P. Grangier, Proposal for a loophole-free bell test using homodyne detection, *Phys. Rev. Lett.* **93**, 130409 (2004).
- [36] S. D. Bartlett and B. C. Sanders, Universal continuous-variable quantum computation: Requirement of optical nonlinearity for photon counting, *Phys. Rev. A* **65**, 042304 (2002).
- [37] R. Birrittella, A. Gura, and C. C. Gerry, Coherently stimulated parametric down-conversion, phase effects, and quantum-optical interferometry, *Phys. Rev. A* **91**, 053801 (2015).
- [38] C. M. Caves, C. Zhu, G. J. Milburn, and W. Schleich, Photon statistics of two-mode squeezed states and interference in four-dimensional phase space, *Phys. Rev. A* **43**, 3854 (1991).
- [39] M. Salvadoray, M. S. Kumar, and R. Simon, Photon distribution in two-mode squeezed coherent states with complex displacement and squeeze parameters, *Phys. Rev. A* **49**, 4957 (1994).
- [40] P. Marian and T. A. Marian, Continuous-variable teleportation in the characteristic-function description, *Phys. Rev. A* **74**, 042306 (2006).
- [41] A. V. Chizhov, L. Knöll, and D.-G. Welsch, Continuous-variable quantum teleportation through lossy channels, *Phys. Rev. A* **65**, 022310 (2002).
- [42] S. L. Braunstein, C. A. Fuchs, and H. J. Kimble, Criteria for continuous-variable quantum teleportation, *Journal of Modern Optics* **47**, 267 (2000).
- [43] S. L. Braunstein, C. A. Fuchs, H. J. Kimble, and P. van Loock, Quantum versus classical domains for teleportation with continuous variables, *Phys. Rev. A* **64**, 022321

- (2001).
- [44] Arvind, B. Dutta, N. Mukunda, and R. Simon, The real symplectic groups in quantum mechanics and optics, *Pramana* **45**, 471 (1995).
- [45] S. L. Braunstein and P. van Loock, Quantum information with continuous variables, *Rev. Mod. Phys.* **77**, 513 (2005).
- [46] G. Adesso and F. Illuminati, Entanglement in continuous-variable systems: recent advances and current perspectives, *J. Phys. A* **40**, 7821 (2007).
- [47] C. Weedbrook, S. Pirandola, R. García-Patrón, N. J. Cerf, T. C. Ralph, J. H. Shapiro, and S. Lloyd, Gaussian quantum information, *Rev. Mod. Phys.* **84**, 621 (2012).
- [48] G. Adesso, S. Ragy, and A. R. Lee, Continuous variable quantum information: Gaussian states and beyond, *Open Syst. Inf. Dyn.* **21**, 1440001, 47 (2014).
- [49] S. Olivares, Quantum optics in the phase space, *The European Physical Journal Special Topics* **203**, 3 (2012).